ATLAS NOTE

ATLAS-CONF-2011-034

March 25, 2011

Measurement of the top quark pair production cross section with ATLAS in pp collisions at $\sqrt{s} = 7$ TeV in dilepton final states

The ATLAS collaboration

Abstract

A measurement is presented of the production cross section of top quark pairs ($\sigma_{t\bar{t}}$) in proton-proton (pp) collisions at $\sqrt{s} = 7$ TeV recorded with the ATLAS detector at the CERN Large Hadron Collider. Using a data sample of 35 pb^{-1}, candidate events are selected in the dilepton topology with large missing transverse energy, $E_{\mathrm{T}}^{\mathrm{miss}}$, and at least two jets. A baseline analysis employing kinematic properties of the candidate events to separate the signal from background and using data-driven techniques to determine the most important backgrounds, results in a measurement of

$$\sigma_{t\bar{t}} = 173 \pm 22(\mathrm{stat.})^{+18}_{-16}(\mathrm{syst.})^{+8}_{-7}(\mathrm{lum.})\ \mathrm{pb},$$

where the three uncertainties are from statistics, systematics and integrated luminosity, respectively. We also perform a cross section measurement requiring at least one b-tagged jet and a looser kinematic selection that increases the signal-to-background ratio, yielding

$$\sigma_{t\bar{t}} = 171 \pm 22(\mathrm{stat.})^{+21}_{-16}(\mathrm{syst.})^{+7}_{-6}(\mathrm{lum.})\ \mathrm{pb}.$$

Additional studies are performed to corroborate these measurements; a technique that normalizes the $t\bar{t}$ signal yield to the measured rate of Z decays, a two-dimensional template shape fit using the $E_{\mathrm{T}}^{\mathrm{miss}}$ vs the number of jets to simultaneously measure the production cross sections of $t\bar{t}$, WW and $Z \to \tau\tau$ final states, and a simultaneous measurement of $\sigma_{t\bar{t}}$ and the b-tagging efficiency using the distribution of the number of tagged jets in each event.

All the measurements are in good agreement with each other and the Standard Model prediction.

1 Introduction

Studies of top quarks produced in proton-proton (pp) collisions at the LHC are becoming an active testing ground for the validity of the Standard Model (SM) [1]. Production of top-antitop quark pairs ($t\bar{t}$) in pp collisions at the LHC is dominated by gg fusion. Within the SM the $t\bar{t}$ production cross section at a centre of mass energy $\sqrt{s} = 7$ TeV is calculated to be 165^{+11}_{-16} pb [2] for a top quark mass of 172.5 GeV. The measurement of the $t\bar{t}$ production cross section ($\sigma_{t\bar{t}}$) in various decay channels allows for a precision test of the predictions of perturbative QCD and a study of the details of top quark decay. The $t\bar{t}$ production process is also an important background for SM Higgs boson searches and in searches for physics beyond the SM. Top quark final states may be a signature for new physics that modify the production and/or decay of top quarks. Finally, $t\bar{t}$ final states can be exploited for understanding and improving aspects of detector performance. Of particular importance is the recognition that $t\bar{t}$ final states provide a pure sample of b-jets in hadron-hadron collisions.

In the SM, the top quark decays to a W boson and a b-quark ($t \to Wb$) nearly 100% of the time, and the $t\bar{t}$ event topologies are determined by the final states of the two W bosons: a pair of quarks, $W \to q\bar{q}$, or a lepton-neutrino pair, $W \to \ell\nu$, where ℓ refers to a lepton. This note focuses on the dilepton channel, in which both W bosons decay to leptons with the final state containing two opposite-sign leptons (ee, $\mu\mu$, $e\mu$), missing transverse energy, $E_{\mathrm{T}}^{\mathrm{miss}}$, which indicates the presence of neutrinos from W boson decays, and two or more jets, including those arising from the b-quarks.

This note is based on ten times more data than the first measurement of $t\bar{t}$ production with the ATLAS detector at the LHC [3] and a $t\bar{t}$ cross section measurement in the dilepton channel performed by CMS [4]. The baseline cross section measurement in the dilepton channel with a straightforward counting method is first described, where a signal-enriched sample is created using kinematic requirements. The background contributions coming from Drell-Yan production and fake lepton candidates are determined using data-driven methods. As an alternative to normalizing the measured event yields to the total inelastic cross section through the luminosity measurement [5], we perform a $\sigma_{t\bar{t}}$ measurement normalizing the $t\bar{t}$ rate to the Z boson production cross section. This also allows partial cancellation of systematic uncertainties on the acceptances. To provide a more global test of the SM in the dilepton final state than that provided by a counting experiment, the dilepton event selection is relaxed with respect to number of jets ($\mathrm{N_{jets}}$) and total transverse energy (H_{T}), and a template shape fit is then used in a two-dimensional $E_{\mathrm{T}}^{\mathrm{miss}}$ vs $\mathrm{N_{jets}}$ space to measure simultaneously the production cross sections of $t\bar{t}$, WW and $Z \to \tau\tau$.

To further suppress backgrounds from processes without b-jets, a second baseline analysis is performed by requiring that at least one of the jets be b-tagged, identified as arising from the decay of a long-lived bottom hadron. This measurement therefore suffers from the additional systematic uncertainty associated with the efficiency of the b-tagging algorithm. We perform a cross-check by simultaneously measuring the b-tagging efficiency and $\sigma_{t\bar{t}}$ by fitting the distribution of the number of b-tagged jets in each event.

2 Detector and data sample

The ATLAS detector [6] at the LHC covers nearly the entire solid angle[1] around the collision point. It consists of an inner tracking detector surrounded by a thin superconducting solenoid, electromagnetic and hadronic calorimeters, and an external muon spectrometer incorporating three large superconducting toroid magnet assemblies. A more detailed description can be found in Ref. [6]. The analyses use

[1] In the right-handed ATLAS coordinate system, the pseudorapidity η is defined as $\eta = -\ln[\tan(\theta/2)]$, where the polar angle θ is measured with respect to the LHC beamline. The azimuthal angle ϕ is measured with respect to the x-axis, which points towards the centre of the LHC ring. The y-axis points up. Transverse momentum and energy are defined as $p_{\mathrm{T}} = p\sin\theta$ and $E_{\mathrm{T}} = E\sin\theta$, respectively.

collision data with a centre of mass energy of $\sqrt{s} = 7$ TeV and an integrated luminosity of $35\,\text{pb}^{-1}$. This luminosity value has a relative uncertainty of 3.4% [5]. Only data where all subsystems described above are operating properly are used.

3 Simulated event samples

Monte-Carlo (MC) simulation samples have been used to develop and validate the analysis procedures, to calculate the acceptance and to evaluate the contributions from specific background processes. After event generation, all samples have been processed with the GEANT4 [7] simulation of the ATLAS detector [8], reconstructed and passed through the same analysis chain as the data.

The generation of $t\bar{t}$, WW and single top events uses the MC@NLO MC program [9] with parton density function (PDF) set CTEQ66 [10] and assuming a top quark mass of 172.5 GeV. The $t\bar{t}$ cross section is normalized using the HATHOR [11] code to 165^{+11}_{-16} pb to take into account next-to-next-to-leading order (NNLO) effects. Single top quark production includes the t, Wt and s channels and the cross section is normalized to the MC@NLO predicted cross section using the 'diagram removal scheme' [12] for the Wt process to remove overlaps with the $t\bar{t}$ final state.

The generation of Z/γ^*+jets (Drell-Yan) events uses the PYTHIA MC generator for the $Z \to \tau\tau$ channel. Events in the $Z/\gamma^* \to ee$ and $Z/\gamma^* \to \mu\mu$ channels are modelled with the ALPGEN v2.13 MC, using the MLM matching scheme [13] with matching parameters RCLUS=0.7 and ETCLUS=20, and using PDF set CTEQ6L1 [14]. The Z/γ^*+jets samples are normalized with an NLO/LO K-factor of 1.25 [15]. For the $t\bar{t}$ cross section measurement with Z normalization, Z/γ^* MC@NLO MC, normalized to the NNLO cross section [16] is used for the inclusive Z analysis. All events are hadronized with HERWIG [17], using the JIMMY underlying event model [18]. Diboson WZ and ZZ events are modelled using the ALPGEN generator, normalized with appropriate NLO/LO K-factors to match the total cross section from NLO QCD calculations made with MCFM [19]. The small background contributions from W+jets production are evaluated using data-driven techniques.

The uncertainties in the kinematic distributions of the $t\bar{t}$ signal events give rise to systematic uncertainties in the analysis through the calculated acceptance, and have contributions from the choice of generator, the amount of initial and final state radiation (ISR/FSR) and PDFs. The uncertainty due to the choice of generator and shower model is evaluated by comparing the predictions of MC@NLO with those of POWHEG [20] interfaced to both HERWIG or PYTHIA. The uncertainty due to ISR/FSR is evaluated by studies using the ACERMC generator [21] interfaced to PYTHIA, and by varying the parameters controlling ISR and FSR in a range consistent with experimental data [15]. Finally, the uncertainty in the PDFs used to generate $t\bar{t}$ and single top events is evaluated using a range of current PDF sets with the procedure described in [15].

For the small backgrounds from single top and diboson production, only overall normalization uncertainties are considered and these are taken to be 10% and 5%, respectively.

4 Object definition and event selection

The event reconstruction makes use of reconstructed electrons, muons, jets, and $E_{\text{T}}^{\text{miss}}$. The latter is sensitive to momentum imbalance in the transverse plane indicating the presence of escaping neutrinos. Various criteria are imposed on these reconstructed objects to perform the baseline event selection.

4.1 Object definition

Electron candidates are required to pass a stringent ('tight') electron selection [22] with $p_{\text{T}} > 20$ GeV and $|\eta_{\text{cluster}}| < 2.47$, excluding the calorimeter crack region at $1.37 < |\eta_{\text{cluster}}| < 1.52$, where η_{cluster} is

the pseudorapidity of the calorimeter energy cluster associated with the candidate. The value of E/p, the ratio of electron cluster energy measured in the calorimeter to momentum in the tracker, must be consistent with that expected for an electron ($0.7 < E/p < 5.0$). In addition, the track must have an associated hit in the innermost pixel layer whenever it passes through an active region in order to suppress backgrounds from photon conversions. High-threshold TRT hits when available are used to help distinguish electrons from other charged particles.

Muon candidates ('tight' muons) are reconstructed by searching for track segments in different layers of the muon chambers. These segments are combined starting from the outermost layer, fitted to account for material effects, and matched with tracks found in the inner detector. The final candidates are refitted using the complete track information from both detector systems, and required to satisfy $p_{\mathrm{T}} > 20$ GeV and $|\eta| < 2.5$.

To reduce backgrounds from fake lepton candidates arising from QCD jets and to suppress the selection of electrons from heavy flavour decays inside jets, the leptons in each event are required to be isolated. For electrons the E_{T} deposited in the calorimeter towers in a cone in η-ϕ space of radius $\Delta R = 0.2$ around the electron position is summed, and the E_{T} associated with the electron candidate is subtracted. The remaining E_{T} is corrected for the p_{T} of the electron (leakage correction) and corrections are applied for the uncorrelated energy flow in the event that would affect the isolation energy measurement. The corrected E_{T} is required to be less than 4 GeV. For muons, the corresponding calorimeter isolation energy in a cone of $\Delta R = 0.3$ is required to be less than 4 GeV, and the analogous sum of track transverse momenta in a cone of $\Delta R = 0.3$ is also required to be less than 4 GeV. Additionally, muons are required to have a distance ΔR greater than 0.4 from any jet with $p_T > 20$ GeV, further suppressing muons from heavy flavour decays inside jets.

Jets are reconstructed with the anti$-k_t$ [23] algorithm with distance parameter R = 0.4 from clustered energy deposits in the calorimeters, calibrated at the electromagnetic (EM) scale appropriate for the energy deposited by electrons or photons. These jets are then calibrated to the hadronic energy scale, using a p_{T} and η dependent correction factor obtained from simulation [24]. Jets are removed if they include the electron candidate cluster. The jet candidates used in the analysis are required to have corrected $p_{\mathrm{T}} > 20$ GeV and $|\eta| < 2.5$.

The $E_{\mathrm{T}}^{\mathrm{miss}}$ is constructed from the vector sum of all calorimeter cells with $|\eta| < 4.5$, projected onto the transverse plane. Cells associated with jets are taken at the corrected energy scale that is used for jets, while the contribution from cells associated with electrons are substituted by the calibrated transverse energy of the electron. Finally, the contribution from muons passing selection requirements is included, also removing the contribution of any calorimeter cells associated to the muon.

4.2 Event selection

The dilepton analysis requires events selected online by a single lepton trigger (e or μ). The detailed trigger requirements vary through the data-taking period, due to the rapidly increasing LHC luminosity and the commissioning of the trigger system, but always with a threshold that guarantees fully-plateaued maximal efficiency for leptons with $p_{\mathrm{T}} > 20$ GeV. For electrons, a level-1 electromagnetic trigger object with a transverse energy threshold varying from 10 to 15 GeV is required. A more refined electromagnetic cluster selection is required in the level-2 trigger. Subsequently, a match between the selected calorimeter electromagnetic cluster and an inner detector track, is imposed in the event filter. Muon candidates are selected by requiring a level-1 muon trigger, which are subsequently confirmed at level-2 and event filter by using the precision chambers of the muon spectrometer. In the later part of the data-taking period, the level-2 and event filter also required that the muon spectrometer track be matched to a track found in the inner detector. The p_{T} threshold used by the event filter varied between 10 and 13 GeV.

To ensure that the event is actually triggered by the leptons used in the analysis, at least one reconstructed lepton and a trigger object are required to match within $\Delta R < 0.15$.

An event is required to have a primary vertex with at least five tracks. Events are discarded if any jet with $p_T > 20$ GeV fails jet quality cuts designed to reject jets arising from out-of-time activity or calorimeter noise [25]. If an electron candidate and a muon candidate (before overlap removal with jets is applied) share a track, the event is discarded.

The selection of events in the signal region consists of a series of kinematic requirements on the reconstructed objects. The $E_{\mathrm{T}}^{\mathrm{miss}}$, the Z mass window, and the H_{T} cuts are derived from a grid scan significance optimization that includes dominant systematic uncertainties, such as jet and lepton energy scale and lepton energy resolution. The resulting event selection is:

- Exactly two oppositely-charged leptons (ee, $\mu\mu$ or $e\mu$) each satisfying $p_{\mathrm{T}} > 20$ GeV, where at least one must be associated to a leptonic high-level trigger object;
- At least two jets with $p_{\mathrm{T}} > 20$ GeV and $|\eta| < 2.5$;
- To suppress backgrounds from Z/γ^*+jets and QCD multi-jet events in the ee and $\mu\mu$ channels, the missing transverse energy must satisfy $E_{\mathrm{T}}^{\mathrm{miss}} > 40$ GeV, and the invariant mass of the two leptons must be at least 10 GeV away from the Z-boson mass of 91 GeV, *i.e.* $|m_{\ell\ell} - m_Z| > 10$ GeV.
- For the $e\mu$ channel, no $E_{\mathrm{T}}^{\mathrm{miss}}$ or Z-mass veto cuts are applied. However, the event H_{T}, defined as the scalar sum of the transverse energies of the two leptons and all selected jets, must satisfy $H_{\mathrm{T}} > 130$ GeV to suppress backgrounds from Z/γ^*+jets production;
- Muon candidates arising from cosmic rays are rejected by eliminating muon candidate pairs with large, oppositely signed transverse impact parameters ($|d_0| > 500$ μm) and consistent with being back-to-back in the $r - \phi$ plane.
- The reconstructed invariant dilepton mass be $m_{\ell\ell} > 15$ GeV in order to reject backgrounds from bottom quark production and vector meson decays.

4.3 Systematic uncertainties on reconstructed objects

The uncertainties due to MC simulation modeling of the lepton trigger, reconstruction and selection efficiencies are assessed using leptons from $Z \to ee$ and $Z \to \mu\mu$ events selected from the same data sample used for the $t\bar{t}$ analyses. Corrections (scale factors) are applied to MC samples when calculating acceptances to account for any observed differences in predicted and observed efficiencies. The statistical and systematic uncertainties on the scale factors are included in the acceptance uncertainties. The modeling of the lepton energy scale and resolution is studied using reconstructed Z-mass distributions, and used to adjust the simulation accordingly.

The jet energy scale (JES) and its uncertainty are derived by combining information from test-beam data, LHC collision data and simulation [24]. The JES uncertainty varies as a function of jet p_{T} and η. The jet energy resolution (JER) and jet finding efficiency measured in data and in simulation are in agreement. The statistical uncertainties of the comparisons, 14% and 2% for the energy resolution and the efficiency, respectively, are taken as the systematic uncertainties.

The b-tagging efficiency ϵ_b is the efficiency that a b-quark jet is tagged by the b-tagging algorithm. Similarly, ϵ_c and ϵ_l are the efficiency of a c-quark jet and light jet to be tagged as a b-jet. These efficiencies are sources of systematic uncertainty when performing an event selection using b-tagging. The performance of the two b-tagging algorithms used in this analysis, JetProb [26] and SV0 [27], has been studied in a similar way to previous measurements using various control samples. The relative uncertainties for the b-tagging efficiency range from 6% to 20%. For light-flavour jets, the simulation underestimates the tagging efficiency by factors ranging from 1.05 to 1.20, with uncertainties on these factors ranging from 8 to 40%.

The LHC instantaneous luminosity varied by several orders of magnitude during this data-taking period, reaching a peak of about 2×10^{32} cm^{-2}s^{-1}. An average of about two extra pp interactions are superimposed on each MC event, which is the average number of extra pp interactions expected in the analyzed data sample. Data-driven determinations of efficiencies and backgrounds naturally include effects of the extra interactions.

5 Backgrounds

The dominant backgrounds come from Z/γ^*+jets production and W+jets production with additional leptons coming from b-quark decays, lighter hadron decays and conversions (non-prompt leptons), and misidentified leptons arising from QCD jets. The term 'fake lepton' will in the following refer to both sources of backgrounds. Both of these backgrounds are estimated from data. The calculation of the fake lepton backgrounds uses a matrix method (Section 5.1). As this background is determined using data-driven techniques, to avoid double-counting MC events when performing acceptance calculations, misidentified leptons are removed from estimates obtained from Monte-Carlo. The calculation of the Z/γ^*+jets background (Section 5.2) is assisted by Monte-Carlo calculations.

The contributions from other small cross section electroweak background processes, such as single top, WW, ZZ and WZ production are estimated from Monte-Carlo simulations.

5.1 Non-Z lepton backgrounds

True $t\bar{t}$ dilepton events contain two leptons from W decays; the background comes predominantly from W+jets events (including the single-lepton $t\bar{t}$ production) with a real and a fake lepton, though there is a smaller contribution with two fake leptons coming from QCD multi-jet production. In the case of muons, the dominant fake-lepton mechanism is a semi-leptonic decay of a heavy-flavour hadron, in which a muon survives the isolation requirement. In the case of electrons, the three mechanisms are heavy flavour decay, light flavour jets with a leading π^0 overlapping with a charged particle, and conversion of photons.

The fraction of the dilepton sample that comes from fake leptons is measured with the matrix method. 'Loose' muons are defined in the same way as tight muons (see Section 4.1), except that the calorimeter and track isolation are relaxed. 'Loose' electrons must fulfill the tight electron cuts (see Section 4.1), except that the requirements on calorimeter isolation, high threshold TRT hits and on E/p are relaxed [3].

The loose lepton selection criteria are then used to count the number of observed dilepton events with two tight, two loose or one tight and one loose leptons (N_{TT}, N_{LL} or N_{TL} and N_{LT}, respectively). Then two probabilities are defined, r (f), to be the probability that real (fake) leptons that pass the loose identification criteria, will also pass the tight criteria. Using r and f, linear expressions are then obtained for the observed yields as a function of the number of events with two real, two fake or one real and one fake leptons (N_{RR}, N_{FF} and N_{RF} or N_{FR}, respectively). The method explicitly accounts for the presence of events with two fake leptons. These linear expressions form a matrix that is inverted in order to extract the real and fake content of the observed dilepton event sample:

$$\begin{bmatrix} N_{TT} \\ N_{TL} \\ N_{LT} \\ N_{LL} \end{bmatrix} = \begin{bmatrix} rr & rf & fr & ff \\ r(1-r) & r(1-f) & f(1-r) & f(1-f) \\ (1-r)r & (1-r)f & (1-f)r & (1-f)f \\ (1-r)(1-r) & (1-r)(1-f) & (1-f)(1-r) & (1-f)(1-f) \end{bmatrix} \begin{bmatrix} N_{RR} \\ N_{RF} \\ N_{FR} \\ N_{FF} \end{bmatrix} \quad (1)$$

The efficiency for a real loose lepton to pass the tight criteria, r, is measured in data in a sample of $Z \to \ell\ell$ events as a function of jet multiplicity. The corresponding efficiency for fake leptons, f, is measured in data in events with a single loose lepton and low $E_{\mathrm{T}}^{\mathrm{miss}}$, which are dominated by QCD di-jet

Non-Z lepton background estimates	N_{jets}	$e\mu$	ee	$\mu\mu$
Matrix method	0	$1.9 \pm 1.0 \pm 1.0$	$1.4 \pm 0.8 \pm 0.7$	$0.0\,^{+0.6}_{-0} \pm 0.3$
Matrix method	1	$3.9 \pm 1.5 \pm 2.0$	$1.9 \pm 0.9 \pm 1.0$	$0.0\,^{+0.6}_{-0} \pm 0.3$
Matrix method	≥ 2	$3.0 \pm 2.1 \pm 1.5$	$0.8 \pm 0.7 \pm 0.4$	$0.5 \pm 0.5 \pm 0.3$
Candidate weighting method	≥ 2	$1.1 \pm 0.6^{+0.3}_{-0.2}$	$0.6 \pm 0.3^{+0}_{-0.1}$	$2.2 \pm 1.1^{+0}_{-0.2}$

Table 1: Overview of the estimated non-Z background yields in the signal and control regions using the matrix method. In the signal region ($N_{\text{jets}} \geq 2$) the method is cross-checked with the candidate weighting method. The matrix method is used as a baseline since it includes contributions from events with two fake leptons, and is less sensitive to potential trigger and $E_{\text{T}}^{\text{miss}}$ bias. Statistical and systematic uncertainties are shown.

production. Contributions from real leptons due to W+jets final states are subtracted using simulated data.

The cross-check comes from comparing results of the matrix method with the 'candidate weighting method'. Isolated tracks (loose electrons) are used as muon (electron) candidates. The rates at which these candidates are identified as muons (electrons) are measured in the inclusive $W \rightarrow \mu\nu$ sample. Events are selected to contain at least one muon and at least one candidate, and to have $E_{\text{T}}^{\text{miss}} > 20$ GeV. To suppress dileptons from Z/γ^*+jets events, the muon and candidate within a pair are required to have the same charge. Known sources of same-sign leptons are subtracted using MC. To estimate the non-Z background, the obtained rates are then applied to the sample containing exactly one good lepton and at least one additional candidate lepton. The dominant uncertainties are due to data statistics.

Table 1 shows the background estimates obtained from the matrix and candidate weighting methods. The two methods are found to agree on the estimated background within their uncertainties.

5.2 Z/γ^*+jets

The $t\bar{t}$ event selection is designed to reject Z/γ^*+jets events. However, a small fraction of such events with large $E_{\text{T}}^{\text{miss}}$ and dilepton invariant mass away from the Z boson mass peak will remain in the signal sample. These events are difficult to properly model in simulations due to large uncertainties on the non-Gaussian $E_{\text{T}}^{\text{miss}}$ tails, on the Z boson cross section for higher jet multiplicities, and on the lepton energy resolution.

To estimate the Z/γ^*+jets background, the number of Z/γ^*+jets events is measured in a control region orthogonal to the $t\bar{t}$ dilepton signal region. The control region (CR) is formed by events with an invariant dilepton mass inside the Z mass window used in the event selection described above, with at least two jets and with $E_{\text{T}}^{\text{miss}} > 30$ GeV. There is contamination in the control region from other physics processes and their contribution is subtracted by relying on the Monte-Carlo prediction. A scale factor is derived using Z/γ^*+jets simulation to extrapolate from the control region into the signal region:

$$\text{N}_{Z/\gamma^*+\text{jets}} = \frac{\text{MC}_{Z/\gamma^*+\text{jets}}(\text{SR})}{\text{MC}_{Z/\gamma^*+\text{jets}}(\text{CR})} \times (\text{Data(CR)} - \text{MC}_{\text{other}}(\text{CR}))\,, \tag{2}$$

where $\text{MC}_{Z/\gamma^*+\text{jets}}(\text{SR/CR})$ represent the number of events in the signal and control region, respectively. The variable MC_{other} is the number of events from other physics backgrounds that contaminate the control region, while Data(CR) represents the observed number of events in the control region.

The robustness of the method is tested by varying the $E_{\text{T}}^{\text{miss}}$ cut in the control region by ±5 GeV, and is referred to as the 'method uncertainty'. The comparison between data-driven and Monte-Carlo methods

Process	ee	$\mu\mu$
Z/γ^*+jets (data-driven)	$1.2^{+0.5}_{-0.6}$	$3.4^{+1.9}_{-1.4}$
Z/γ^*+jets (Monte-Carlo)	$2.8^{+3.1}_{-1.8}$	$3.4^{+4.1}_{-2.4}$

Table 2: Yields and total uncertainties for the estimates of the Z/γ^*+jets background with data-driven and Monte-Carlo methods.

demonstrates that data-driven normalization using the control regions helps to reduce the effect of the systematic uncertainties. The number of Z/γ^*+jets background events from this data-driven method is summarized in Table 2 for the ee and $\mu\mu$ channels. The most important uncertainties on the estimation are shown in Table 3 for the ee and $\mu\mu$ channel, respectively.

Uncertainty(%)	ee (DD)	ee (MC)	$\mu\mu$ (DD)	$\mu\mu$ (MC)
Data statistics	+34/-27	-	+14/-13	-
Jet energy scale	+8/-16	+104/-51	-23/+45	+114/-57
Jet energy resolution	±7	±22	±6	±13
Monte-Carlo cross section	-4/+7	±29	+4/-9	±38
Monte-Carlo statistics	±18	±17	±15	±15
Muon momentum resolution	-	-	+3/-5	+3/-5
Method (see text)	±27	-	±22	-
total (syst + lumi + stat)	±46	+112/-66	+56/-41	+122/-72

Table 3: Dominant (and total) uncertainties on the predicted number of Z/γ^*+jets events in the signal region from data statistics, jet energy scale, jet energy resolution, theoretical MC cross sections, MC statistics and lepton energy resolutions. The uncertainty due to the method is evaluated from the variation of the prediction when the $E_{\mathrm{T}}^{\mathrm{miss}}$ cut in the control region is varied by ±5 GeV. The uncertainties are compared between the data-driven (DD) determination and the determination from Monte-Carlo simulations. The uncertainties of the prediction are presented as +1 σ / -1 σ variation of the systematic source.

5.3 Control samples

The modeled acceptances, efficiencies and data-driven background estimate methods are validated by comparing Monte-Carlo simulations with data in control regions which are depleted of $t\bar{t}$ events, but have similar kinematics. Figure 1 (a) and (d) show $E_{\mathrm{T}}^{\mathrm{miss}}$ for events inside the Z mass region and with at least 2 jets, (b) and (e) show the jet multiplicity for events where the dilepton mass lies inside the Z boson peak and $E_{\mathrm{T}}^{\mathrm{miss}} < 40$ GeV. This tests the initial state radiation (ISR) modeling of jets for Z/γ^*+jets processes. The dilepton mass plots, Figure 1 (c) and (f), probe the lepton energy scale and resolution.

6 Cross section measurement

A baseline analysis employing kinematic properties of the candidate events is described in Section 6.1. Additional studies performed to corroborate these measurements are described in Section 6.2.

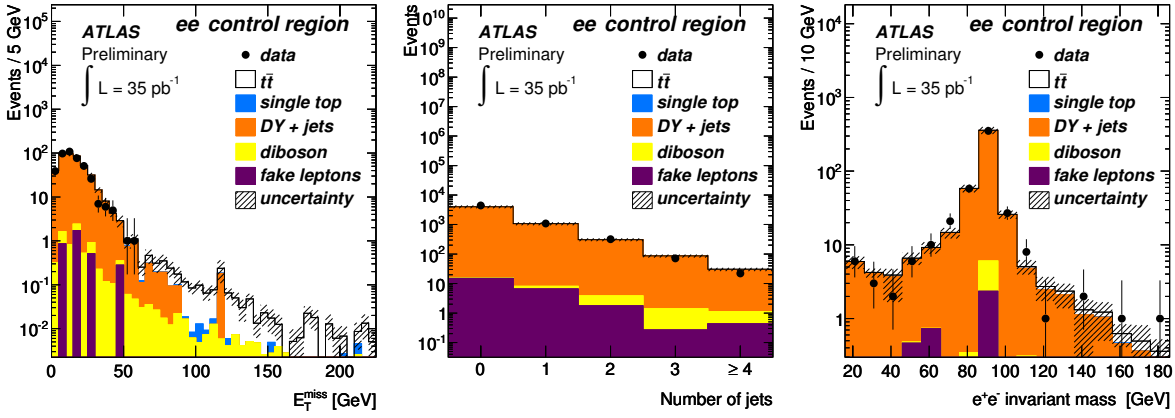

(a) $E_{\mathrm{T}}^{\mathrm{miss}}$ (ee) (b) $\mathrm{N}_{\mathrm{jets}}$ (ee) (c) Lepton pair mass (ee)

(d) $E_{\mathrm{T}}^{\mathrm{miss}}$ ($\mu\mu$) (e) $\mathrm{N}_{\mathrm{jets}}$ ($\mu\mu$) (f) Lepton pair mass ($\mu\mu$)

Figure 1: Control region distributions for the counting method analysis without b-tagging. Top row ee, bottom row $\mu\mu$: (a),(d) $E_{\mathrm{T}}^{\mathrm{miss}}$ in events with dilepton mass $m_{\ell\ell}$ inside the Z mass window with ≥ 2 jets, (b),(e) the number of jets in events with $m_{\ell\ell}$ inside the Z mass window and $E_{\mathrm{T}}^{\mathrm{miss}} < 40$ GeV and (c),(f), the $m_{\ell\ell}$ of opposite-sign lepton pairs in events with $\geq$2 jets in the low $E_{\mathrm{T}}^{\mathrm{miss}}$ region. The error bands reflect the statistical and systematic uncertainties of the MC prediction.

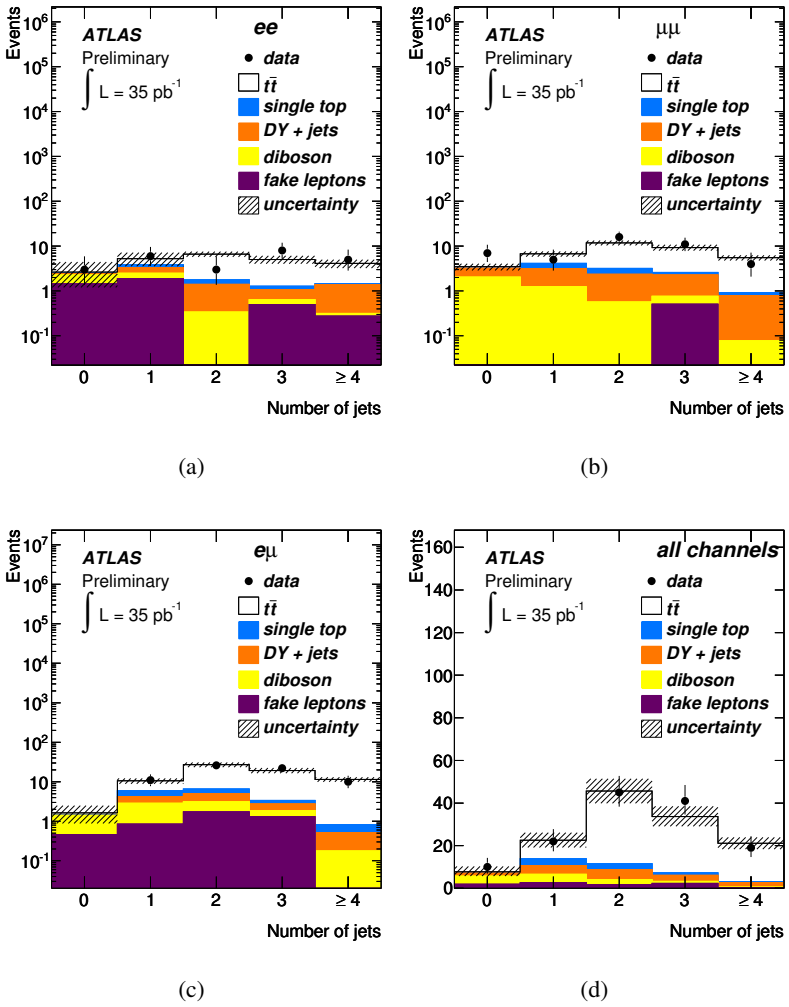

Figure 2: Jet multiplicity distributions for the counting method in the signal region omitting the $N_{jets} \geq 2$ requirement in (a) the *ee* channel, (b) the $\mu\mu$ channel, (c) the $e\mu$ channel and (d) combined.

6.1 Counting method

The cross section measurement is a counting experiment where the excess of signal candidates above background is corrected for acceptance. Drell-Yan and fake lepton backgrounds are estimated from data and the other backgrounds are estimated from simulation.

6.1.1 Event yields

The expected and measured numbers of events in the signal region after applying all selection cuts as described in Section 4.2 for each of the individual dilepton channels are shown in Table 4. A total of 105 candidate events are observed, 16 in the *ee*-channel, 31 in the $\mu\mu$-channel and 58 in the $e\mu$-channel.

The predicted and observed multiplicities of selected jets are compared in Figure 2 for each channel individually and for all channels combined. Figure 3 shows the predicted and observed distributions of $E_{\mathrm{T}}^{\mathrm{miss}}$ for the *ee* and $\mu\mu$ channels and of H_{T} for the $e\mu$ channel. In general there is good agreement between the background model and the data.

From the measured missing transverse energy, and the transverse momenta of the leptons and jets,

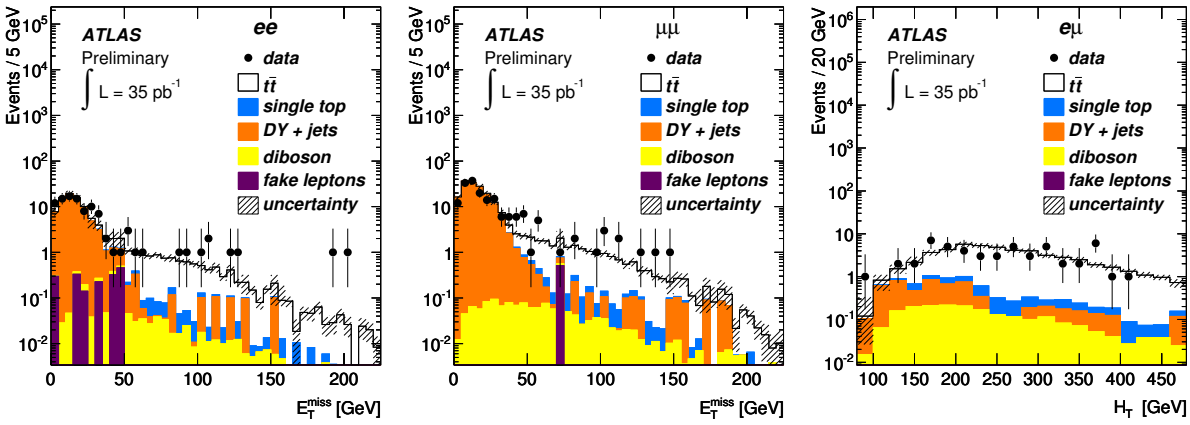

(a) (b) (c)

Figure 3: $E_{\mathrm{T}}^{\mathrm{miss}}/H_{\mathrm{T}}$ distributions for the counting method in the signal region. The $E_{\mathrm{T}}^{\mathrm{miss}}$ distribution is shown for (a) the ee channel and for (b) the $\mu\mu$ channel without the $E_{\mathrm{T}}^{\mathrm{miss}} > 40$ GeV requirement, and (c) H_{T}, defined as the scalar sum of the transverse energies of the two leptons and all selected jets, is shown without the $H_{\mathrm{T}} > 130$ GeV requirement.

	ee	$\mu\mu$	$e\mu$
Z/γ^*+jets (DD)	$1.2^{+0.5}_{-0.6}$	$3.4^{+1.9}_{-1.4}$	-
$Z(\rightarrow \tau\tau)$+jets (MC)	$0.4^{+0.4}_{-0.3}$	$1.2^{+0.7}_{-0.6}$	$3.2^{+1.6}_{-1.3}$
Non-Z leptons (DD)	0.8 ± 0.8	0.5 ± 0.6	3.0 ± 2.6
Single top (MC)	0.7 ± 0.1	1.3 ± 0.2	2.5 ± 0.4
Dibosons (MC)	0.5 ± 0.1	0.9 ± 0.2	$2.1^{+0.5}_{-0.3}$
Total (non $t\bar{t}$)	3.5 ± 1.1	$7.3^{+1.8}_{-1.5}$	10.8 ± 3.4
$t\bar{t}$ (MC)	11.5 ± 1.3	20.1 ± 1.7	47.4 ± 4.0
Total expected events	15.0 ± 1.7	27.4 ± 2.4	58.2 ± 5.2
Observed events	16	31	58

Table 4: Full breakdown of the expected $t\bar{t}$-signal and background in the signal region compared to the observed event yields, for each of the dilepton channels (MC is simulation based, DD is data driven). All systematic uncertainties are included, and correlations between different background sources are taken into account.

the transverse mass variable m_{T2} [28] is constructed for each selected event. It is defined as

$$m_{\mathrm{T2}}^2 = \min_{\not{p}_{(1)}+\not{p}_{(2)}=E_{\mathrm{T}}^{\mathrm{miss}}} \left[\max\{m_{\mathrm{T}}^2(p_{\mathrm{T}}^{lj(1)}, \not{p}_{(1)}), m_{\mathrm{T}}^2(p_{\mathrm{T}}^{lj(2)}, \not{p}_{(2)})\}\right]$$

where

$$m_{\mathrm{T}}^2(p_{\mathrm{T}}^{lj(i)}, \not{p}_{(i)}) = m_{lj(i)}^2 + m_{\not{p}_{(i)}}^2 + 2[E_{\mathrm{T}}^{lj(i)} E_{\mathrm{T}}^{\not{p}_{(i)}} - \vec{p}_{\mathrm{T}}^{\,lj(i)} \vec{p}_{\mathrm{T}}^{\,\not{p}_{(i)}}]$$

and

$$E_{\mathrm{T}} = \sqrt{m^2 + p_{\mathrm{T}}^2}$$

with the transverse momentum of the composite object of one lepton and one jet $p_{\mathrm{T}}^{lj(i)}$, of the trial neutrino $\not{p}_{(i)}$ and their transverse energy E_{T} and masses m. The minimization uses trial momenta for the neutrinos which only have to satisfy the measured $E_{\mathrm{T}}^{\mathrm{miss}}$. From the two possible combinations of leptons and highest-p_{T} jets the combination with the smallest m_{T2} is chosen. The kinematic features observed in Figure 4 are compatible with those expected for dileptonic top quark pair production.

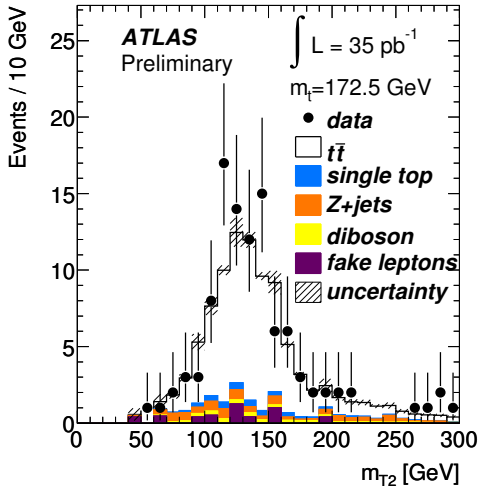

(a)

Figure 4: The m_{T2} distributions for events that pass the selection criteria in the three dilepton channels.

6.1.2 Cross section determination and combination of channels

The observed event count for each channel $\mathrm{N}^{\mathrm{obs}}$ is modeled as being Poisson distributed about some expectation $\mathrm{N}_{\mathrm{tot}}^{\mathrm{exp}}$, which is the sum of several contributions from signal and background processes. The variation in the expected number of events from each process due to systematic uncertainties is parametrized and additional terms are included into a likelihood function that summarizes the uncertainty in the corresponding nuisance parameters. The signal expectation is scaled according to the luminosity, and the signal cross section, σ_{sig}, the parameter of interest, is a free parameter in the fit.

The various systematic uncertainties are organized according to their sources. Most sources of the systematic uncertainties are clearly uncorrelated, for example the muon identification efficiency and the jet energy scale. In more complicated cases, such as heavy flavour content, the independent sources are diagonalized such that the new sources can be considered totally uncorrelated. For each source of systematic (indexed by j) a nuisance parameter α_j is introduced, such that $\alpha_j = 0$ represents the nominal estimate and $\alpha_j = \pm 1$ represents a $\pm 1\sigma$ variation of that source. Next, the sources of the systematics are varied (e.g. jet energy scale, trigger efficiencies, etc.) and a piecewise-linear interpolation is used to parametrize the expected number of events $N_i^{\mathrm{exp}}(\vec{\alpha})$ for each signal and background. A change in the source of the j^{th} systematic introduces a totally correlated variation in the signal and backgrounds.

Additional terms are added to the likelihood function to summarize our knowledge of the α_j derived from auxiliary measurements or assumptions about the uncertainty in the Monte-Carlo modeling. This

leads to the final form of the likelihood function:

$$\mathcal{L}(\sigma_{\mathrm{sig}}, L, \alpha_j) = \prod_{i \in \text{ channel}} \mathrm{Pois}\left(N_i^{\mathrm{obs}} \,|\, N_{i,\mathrm{tot}}^{\mathrm{exp}}(\vec{\alpha})\right) \times G(L_0|L, \sigma_L) \times \prod_{j \in \mathrm{syst}} G(0|\alpha_j, 1)\,, \tag{3}$$

where L_0 is the nominal integrated luminosity. The cross section is inferred from the profile likelihood ratio $\lambda(\sigma_{sig}) = \mathcal{L}(\sigma_{sig}, \hat{\hat{L}}, \hat{\hat{\alpha}}_j)/\mathcal{L}(\hat{\sigma}_{sig}, \hat{L}, \hat{\alpha}_j)$, where a single circumflex represents the maximum likelihood estimate (MLE) of the parameter and the double circumflex represents the conditional MLE with σ_{sig} fixed. Ensembles of pseudo-data were generated for $\mathrm{N_i^{obs}}$ and the resulting estimate of $\hat{\sigma}_{sig}$ was confirmed to be unbiased. Additionally, the variance of $\hat{\sigma}_{sig}$ was found to be consistent with the curvature of the profile likelihood at its minimum.

Uncertainty (%)	*ee*	$\mu\mu$	$e\mu$	Combined	*ttZ*
Data Statistics	-32 / 38	-26 / 29	-15 / 17	-13 / 13	-12 / 13
Luminosity	-3 / 5	-3 / 6	-4 / 4	-4 / 5	N/A
MC Statistics	-3 / 4	-2 / 5	-2 / 2	-2 / 2	-2 / 2
e/μ Energy Scale (ES)	0 / 0	0 / 1	0 / 0	0 / 1	-1 / 1
e/μ Energy Resolution (ER)	0 / 0	0 / 2	0 / 0	0 / 0	-1 / 1
e/μ Scale Factor (SF)	0 / 10	0 / 2	-4 / 5	-4 / 4	-1 / 1
Jet Energy Scale (JES)	-10 / 13	0 / 3	-6 / 4	-5 / 4	-5 / 4
JER	0 / 2	0 / 1	0 / 0	0 / 0	-1 / 1
JEF	0 / 3	-1 / 4	-2 / 2	-2 / 2	-2 / 2
DY Method	-4 / 5	-5 / 4	0 / 0	-2 / 1	-2 / 1
Fake	-7 / 7	-2 / 4	-6 / 5	-4 / 3	-4 / 3
Generator	0 / 3	0 / 1	-2 / 2	-1 / 2	-2 / 1
Parton Shower	-4 / 8	0 / 4	-4 / 5	-4 / 5	-4 / 4
ISR	-3 / 2	0 / 3	0 / -3	-1 / 0	-2 / 1
FSR	-3 / 3	-7 / 0	-2 / 0	-2 / 2	-2 / 2
PDF	-1 / 4	0 / 4	-2 / 3	-2 / 3	-2 / 2
Pile-up	-1 / 3	0 / 2	-1 / 0	0 / 1	-1 / 1
MC Cross Section	0 / 4	-1 / 4	-3 / 2	-2 / 2	-2 / 2
Z Theory	N/A	N/A	N/A	N/A	-7 / 8
All Syst. but Lumi.	-15 / 21	-8 / 10	-10 / 11	-9 / 10	-11 / 12
All Systematics	-15 / 21	-9 / 11	-11 / 12	-10 / 12	-11 / 12
Stat. + Syst.	-35 / 43	-28 / 31	-19 / 21	-16 / 18	-16 / 17

Table 5: Overview of the $t\bar{t}$ cross section uncertainties from the individual channels and from the combination. The cross section measurement with Z normalization (*ttZ*) is described in Section 6.2.1. The uncertainties include statistical uncertainties from data and MC, luminosity uncertainties, uncertainties on the lepton/jet energy scale ('ES'), the energy resolution ('ER'), the lepton scale factor ('SF') and the jet efficiency ('JEF'), uncertainties from the data-driven Z/γ^*+jets ('DY Method') and fake estimation ('Fake'), uncertainties from the choice of the MC generator ('Generator') and parton shower model, initial and final state radiation ('ISR/FSR'), parton density functions ('PDF'), theoretical cross section uncertainties of backgrounds estimated from MC and the uncertainty on the theoretical *Z* cross section ('Z Theory', only applicable to the *ttZ* analysis). They are described in Section 4.3. All uncertainties are relative to the central value of the cross section.

Table 5 provides the systematic uncertainties for each contribution. The largest sources of systematic uncertainty come from the jet energy scale, the fake lepton estimates and the parton shower model employed in the MC calculations. Table 6 summarizes the cross sections extracted from the profile likelihood ratio for the individual channels and for the combination of all three channels.

Channel	$\sigma_{t\bar{t}}$ (pb) (stat., syst., lum.)
ee	$178\ ^{+67\ +37\ +9}_{-57\ -27\ -5}$
$\mu\mu$	$194\ ^{+57+20\ +12}_{-51-15\ -5}$
$e\mu$	$164 \pm 26 \pm 18\ ^{+7}_{-6}$
combined	$173 \pm 22^{+18\ +8}_{-16\ -7}$

Table 6: Measured cross sections in each individual dilepton channel, and the all three channels combined. The uncertainties are obtained from the likelihood minimization.

6.2 Cross-checks

In this section two cross-checks to the counting method are presented: a $\sigma_{t\bar{t}}$ measurement normalizing the $t\bar{t}$ rate to the Z production cross section (Section 6.2.1), and a template shape fit in the two-dimensional $E_{\mathrm{T}}^{\mathrm{miss}}$ vs $\mathrm{N_{jets}}$ parameter space to measure simultaneously the production cross sections of $t\bar{t}$, WW and $Z \to \tau\tau$ (Section 6.2.2).

6.2.1 Cross section measurement with Z normalization

The standard method for extracting the cross section uses the luminosity measurement as a normalization. An alternative method is to normalize the measured $\sigma_{t\bar{t}}$ to a theoretically well understood high energy process, such as Z boson production. This can be achieved by performing an inclusive Z boson analysis in the same dataset as used for the counting analysis. $\sigma_{t\bar{t}}$ can be extracted by performing a combined fit to the five analysis channels ($t\bar{t} \to ee, e\mu, \mu\mu; Z \to ee, \mu\mu$), where the free parameters are $\sigma_{t\bar{t}}$ and $\int \mathcal{L}dt$. In this way the luminosity (and its uncertainty) used in the standard analysis is replaced with the theoretical prediction and associated uncertainty on the Z boson production cross section. This technique is similar to the ratio measurement of $\sigma_{t\bar{t}}/\sigma_Z$ performed by CDF [29]; however in that analysis the luminosity was still used as an input to normalize some background processes.

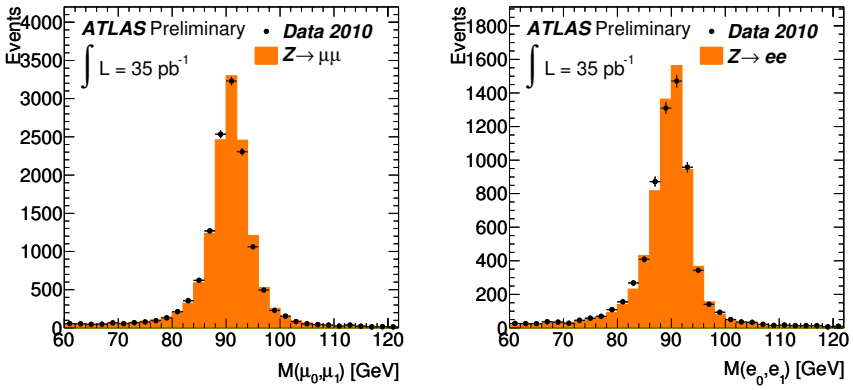

(a) (b)

Figure 5: Dilepton invariant mass distributions before the Z window requirement (see text) is made for (a) $\mu\mu$ events and (b) ee events. Non-Z backgrounds are negligible.

Z boson candidate events are selected by requiring exactly two electrons or muons that pass the same selection criteria as described in Section 4.1. To ensure that the Z boson selection is orthogonal to the

$t\bar{t}$ selection, the mass of the selected dilepton system is required to fall within the Z mass window used as a veto in the $t\bar{t}$ candidate event selection. The dilepton mass distribution before the selection is shown in Figure 5, and illustrates good agreement between the data, where we observe 6048 $Z \to ee$ and 12525 $Z \to \mu\mu$ candidate events, and the expectation from the MC simulation.

Systematic Source, systematic uncertainties in %	$Z \to ee$	$Z \to \mu\mu$
Electron energy / Muon momentum scale	$^{+0.5}_{-1.2}$	± 0.10
Electron energy / Muon momentum resolution	$^{+0.04}_{-0.05}$	$^{+0.07}_{-0.12}$
Electron / Muon identification efficiencies	± 5.3	± 1.6
Electron / Muon trigger efficiencies	$^{+0.9}_{-1.1}$	± 0.26
Theoretical cross section	± 5	± 5
MC Modeling	± 4	± 4

Table 7: Summary of systematic uncertainties (in %) in the inclusive Z boson analysis used in the $t\bar{t}$ cross section measurement with Z normalization.

Uncertainties on PDFs and on the MC modeling of Z production lead to an uncertainty of 4% on the efficiency to select the Z events, while the uncertainty on the theoretical inclusive Z production cross section is taken as 5% [22]. The systematic uncertainties for this analysis are summarized in Table 7.

We have measured the ratio $r = n_{Z\to\ell\ell}/n_{t\bar{t}\to\ell\ell}$ where $n_{Z\to ll}$ is the number of Z boson events observed in the Z analysis and $n_{\bar{t}t\to ll}$ is the number of signal events observed in the top-pair analysis. In the same-flavour lepton channels the equivalent same-flavour Z selection is used for the ratio. In the $e\mu$ channel, $n_{Z\to ll} = 2\times\sqrt{n_{Z\to ee}\times n_{Z\to\mu\mu}}$ is used. The measured ($r^{\rm d}$) and expected values ($r^{\rm e}$) for the three $t\bar{t}$ channels are $r^{\rm d}_{ee} = 476 \pm 170$, $r^{\rm e}_{ee} = 524^{+75}_{-78}$, $r^{\rm d}_{\mu\mu} = 517 \pm 138$, $r^{\rm e}_{\mu\mu} = 623^{+75}_{-87}$, $r^{\rm d}_{e\mu} = 361 \pm 69$, and $r^{\rm e}_{e\mu} = 368^{+46}_{-53}$, where the quoted errors include both statistical and systematic uncertainties.

In order to derive $\sigma_{t\bar{t}}$, the likelihood function described in Section 6.1.2 is extended by adding terms to describe the Z boson analysis. The lepton related uncertainties are correlated with the relevant uncertainties in the $t\bar{t}$ analysis and this allows them to be constrained in the fit. The top-pair production cross section and integrated luminosity are simultaneously measured from the fit to the data to yield

$$\sigma_{t\bar{t}} = 178 \pm 22\ (\text{stat.}) \pm 20\ (\text{syst.})\ \text{pb} \quad (4)$$

$$\int \mathcal{L}dt = 34.5^{+2.4}_{-2.1}\ \text{pb}^{-1}. \quad (5)$$

These are in good agreement with the SM prediction and the standard ATLAS luminosity determination. The total uncertainty on the $t\bar{t}$ production cross section is comparable to the result obtained when using only the $t\bar{t}$ analysis and it is shown in Table 5.

6.2.2 An inclusive dilepton analysis

A second cross-check is provided by using an inclusive dilepton analysis technique to measure simultaneously the production cross sections of $t\bar{t}$, WW and $Z \to \tau\tau$ in the dilepton final state. This analysis is similar to the dilepton counting analysis (Section 6.1), except that a template shape fit is used instead of counting events, and the selection is relaxed with respect to number of jets and $H_{\rm T}$. For the ee and $\mu\mu$ channels which suffer from an overwhelming Drell-Yan contribution, the cuts on $E^{\rm miss}_{\rm T}$ and $m_{\ell\ell}$ (see Section 4.2) are retained. Table 8 summarizes the expected and observed yields before the fit.

The spirit of the technique is to provide a test of the SM predictions in the dilepton final state. As seen in Table 4, the dominant processes with real leptons contributing to the $e\mu$ final state are $t\bar{t}$, WW

Process	$e\mu$	ee	$\mu\mu$
$t\bar{t}$	53.2 ± 4.6	12.3 ± 1.0	22.6 ± 1.9
$Z \to \tau\tau$	44.9 ± 6.7	0.8 ± 0.5	1.6 ± 0.8
WW	12.5 ± 3.0	1.8 ± 0.4	4.1 ± 0.9
Fake leptons	34.2 ± 17	4.1 ± 2.0	0.5 ± 0.3
$Z\gamma$+ jets	1.5 ± 0.8	2.3 ± 1.0	5.3 ± 2.6
Single top	4.4 ± 0.7	1.1 ± 0.2	2.2 ± 0.3
WZ, ZZ	0.9 ± 0.2	0.3 ± 0.1	0.5 ± 0.1
Total predicted	151.6 ± 19	22.8 ± 2.5	36.8 ± 3.5
Observed	146	26	47

Table 8: The expected and observed yields before the template fit to the cross sections for $t\bar{t}$, WW and $Z \to \tau\tau$ final states (inclusive analysis). All systematic uncertainties are included.

and $Z \to \tau\tau$, each of which has distinct missing transverse momentum ($E_{\mathrm{T}}^{\mathrm{miss}}$) and jet multiplicity ($\mathrm{N_{jets}}$) characteristics. Typical $t\bar{t}$ events have large $E_{\mathrm{T}}^{\mathrm{miss}}$ and large $\mathrm{N_{jets}}$. WW events usually have large $E_{\mathrm{T}}^{\mathrm{miss}}$ and relatively low $\mathrm{N_{jets}}$, while $Z \to \tau\tau$ events tend to have low $E_{\mathrm{T}}^{\mathrm{miss}}$ and smaller $\mathrm{N_{jets}}$. Therefore, the two-dimensional parameter space defined by $E_{\mathrm{T}}^{\mathrm{miss}}$ and $\mathrm{N_{jets}}$ is used to naturally separate these main contributions, and fit the observed data to Monte-Carlo generated templates of all expected processes. The normalizations of the main processes described vary as parameters in the fit, allowing a simultaneous measurement of their cross sections. The other 'background' contributions are included with fixed normalizations. The background shapes and acceptances, and other quantities such as lepton and trigger efficiencies, are estimated using a combination of Monte-Carlo and data-driven techniques. The $e\mu$ channel is fitted first, and then the $e\mu$, ee and $\mu\mu$ channels are combined in a single fit.

The results from the analysis are summarized in Table 9. The first row shows the cross sections and the associated uncertainties from the fit performed using the $e\mu$ channel only. Additional statistical information, primarily for $t\bar{t}$, is available also in the ee and $\mu\mu$ channels. The results from the combined fit to all three channels are shown in the second row, including statistical, systematic and integrated luminosity uncertainties. The third row lists the theoretical prediction. The measurement agrees with baseline analysis and expectation. [2]

	$\sigma_{t\bar{t}}$ [pb]	σ_{WW} [pb]	$\sigma_{Z\to\tau\tau}$ [pb]	$\sigma_{t\bar{t}}$ [pb] (Z & WW fixed)
$e\mu$	163±28±14±6	46±26±9±2	1400±290±160±40	164±27±14±5
All channels	171±22±14±5	59±21±12±2	1400±290±160±40	173±21±14±5
Theory	165^{+11}_{-16}	$46.2^{+2.3}_{-2.3}$	1076^{+54}_{-54}	165^{+11}_{-16}

Table 9: Summary of measured cross sections. They are compared to previous measurements and those predicted by theory. The last column has $Z \to \tau\tau$ and WW cross sections constrained to the theoretical predictions within 15%.

[2]Recent studies of the WW production cross section have been performed by the ATLAS [30] and CMS collaborations [31] and are compatible with the results presented here.

7 Cross section measurement using b-tagging information

The $t\bar{t}$ dilepton channel has the largest signal-to-background ratio (S/B) of all the $t\bar{t}$ decay modes. The requirement of the presence of a b-tagged jet further improves the S/B in the sample, reduces some of the systematic uncertainties and provides further confirmation that the event sample is dominated by the expected $t\bar{t}$ final states of two W bosons and two b-jets. The effectiveness of this strategy is limited by the efficiency (ϵ_b) of the b-tagging algorithms and the uncertainties on the b-tagging efficiency and rejection.

We demand at least one b-tagged jet as an additional requirement as our b-tagging baseline measurement. Because of the significantly improved S/B that arises from this requirement, the event selection is modified to increase the efficiency of the selection. A cross check of this measurement is a technique that counts the number of b-tagged candidates in the sample and uses the distribution of the number of b-tagged jets per event to measure simultaneously the $t\bar{t}$ cross section and the b-tagging efficiency.

7.1 B-tagging algorithms

The long lifetime of b-hadrons and the typical boost of a b-jet in a top quark decay result in jets that contain secondary decays that are well-separated from the primary interaction. The precision tracking in the ATLAS detector enables these jets to be "b-tagged" at relatively high efficiency. ATLAS has developed a number of b-tagging algorithms that employ this secondary vertex technique, each with a range of operating points that enable one to select a b-tagging algorithm and operating point with a given overall efficiency and light quark and gluon jet rejection.

In this study, the JetProb and SV0 algorithms [26, 27] are employed. The JetProb algorithm takes all the well-measured tracks associated with a given jet and forms a combined p-value for those tracks to all be coming from the primary interaction vertex. Typically, a b-jet has a number of displaced tracks arising from the b-decay that would be inconsistent with coming from the primary interaction resulting in a low p-value for the jet. A selection based on the p-value forms the basis for this algorithm. Studies have shown that this algorithm can have b-tagging efficiencies as high as 70-80% per jet with light quark and gluon rejections of order one hundred. The SV0 algorithm searches for secondary vertices displaced from the primary interaction. It is expected to have better rejection against light quark and gluon jets but it does not have the same range of efficiencies as the JetProb algorithm.

7.2 Counting method

We employ a direct counting method using a kinematic selection of candidate events with the additional requirement of at least one b-tagged jet. The baseline dilepton event selection without b-tagging, described in Section 6.1, produces a sample with expected signal-to-background (S/B) of ≈ 3.5. This can be improved by requiring at least one b-tagged jet using the JetProb algorithm. We studied the figure of merit $F_M \equiv S/\sqrt{S+B}$, and optimized the event selection for the baseline b-tagging measurement.

Given the size of the current event sample and expected backgrounds, a b-tagging operating point with an efficiency of approximately 70% per jet and light quark and gluon jet rejection factors above 100, maximizes F_M over a broad range of possible event selection criteria. With this choice of b-tagging operating point, we relax some of the kinematic event selection requirements to further increase F_M. In particular, the Z boson veto for the ee and $\mu\mu$ channels is modified by reducing the mass window veto from ± 10 GeV around the Z boson mass to a window of ± 5 GeV, and the $E_{\mathrm{T}}^{\mathrm{miss}}$ and H_{T} requirements were modified to $E_{\mathrm{T}}^{\mathrm{miss}} > 30$ GeV and $H_{\mathrm{T}} > 110$ GeV.

The backgrounds to this selection are estimated using the techniques described in Section 6.1, where no b-tagging requirements were imposed. The dominant backgrounds come from Drell-Yan (ee and $\mu\mu$) production and W production with additional non-prompt (mostly from b-quark decays) and fake lepton candidates in the event. These are estimated by a combination of MC and data-driven techniques in

Process	Event Yields		
	ee	$\mu\mu$	$e\mu$
Z/γ^*+ jets	$1.5^{+1.4}_{-1.0}$	5.2 ± 2.5	N/A
$Z(\rightarrow \tau\tau)$+jets	0.2 ± 0.2	0.3 ± 0.2	0.7 ± 0.5
Fake leptons	0.5 ± 0.5	0.5 ± 0.5	1.9 ± 1.1
Single top	0.6 ± 0.1	1.2 ± 0.2	1.9 ± 0.4
Dibosons	0.2 ± 0.1	0.2 ± 0.1	0.4 ± 0.1
Total Predicted Backgrounds	$2.9^{+1.5}_{-1.1}$	7.4 ± 2.6	5.0 ± 1.3
Predicted $t\bar{t}$ Signal	12.1 ± 1.4	$21.9^{+1.9}_{-2.2}$	$41.4^{+3.5}_{-3.9}$
Total Predicted	15.0 ± 1.9	29.3 ± 3.3	$46.4\ ^{+3.7}_{-4.1}$
Data	15	32	46

Table 10: The expected and observed event yields after requiring at least one b-tagged jet and using an optimized kinematic selection.

the same manner as described in Section 6, now taking into account the additional effect of b-tagging. Modeling of fake lepton backgrounds was done using the matrix method described in Section 5.1. The background estimates are listed in Table 10.

This analysis has some of the same sources of systematic uncertainty as the non b-tagging analysis, and these have been estimated in the same way. The only additional source of systematic uncertainty arises from the uncertainty in the efficiencies of the JetProb tagging algorithm. This has been estimated to be approximately +6% and −8% for b-quark jets, based on b-tagging calibration studies using inclusive lepton and multijet final states. The uncertainties on the tagging effiiciencies for light and charm quarks are several times higher, but are not a large source of uncertainty due to the intrinsically high S/B ratios in the dilepton final state. The systematic uncertainties are summarized in Table 11 for each channel, along with the statistical uncertainties.

The expected event yields from the processes that contribute to this final state are summarized in Table 10, along with the events that satisfy the looser kinematic selection and that there be at least one b-tagged jet. The largest backgrounds in the ee and $\mu\mu$ channel come from Z/γ^*+ jets production. The next largest background comes from single top production and has been estimated using the MC calculations described in Section 3.

These estimates result in $\approx$ 15 background events and $\approx$ 75 events from $t\bar{t}$ production, assuming a $t\bar{t}$ production cross section of 165 pb. This is consistent with the observed yield of 93 candidate events. The expected S/B of this sample has increased to $\approx$ 5, reflecting a significant improvement over the $S/B \approx 3.5$ obtained with the kinematic cuts described in Section 6 for the counting analysis without b-tagging. Note that the expected $t\bar{t}$ signal is only $\approx$ 5% less than in the analysis without b-tagging.

The characteristics of the resulting event sample are consistent with the background and signal estimates, as shown in Figure 6 where we plot the distributions of $E_{\mathrm{T}}^{\mathrm{miss}}$ for the ee and $\mu\mu$ channels, and the H_{T} distribution for the $e\mu$ channel. A likelihood fit is performed to extract a measured $t\bar{t}$ cross section and the results are shown in Table 12.

7.3 Cross-check: Simultaneous measurement of the b-tagging efficiency and $\sigma_{t\bar{t}}$

We use the $t\bar{t}$ candidate events to directly measure the fraction of jets that are successfully tagged as b-jets and simultaneously measure the $t\bar{t}$ production cross section. This serves as a cross-check on the results presented in the previous subsection as it does not rely on the estimates of the b-tagging efficiency

	ee	$\mu\mu$	$e\mu$	combined
Uncertainty Source	$\Delta\sigma/\sigma$[%]	$\Delta\sigma/\sigma$[%]	$\Delta\sigma/\sigma$[%]	$\Delta\sigma/\sigma$[%]
Data Statistics	+35/29	+28/-24	+17/-16	+13/-12
Luminosity	+ 5/- 3	+ 4/- 4	+ 4/- 3	+ 4/- 3
MC Statistics	+ 2/- 3	+ 3/- 5	+ 1/- 1	+ 2/- 1
e/μ Energy Scale	+ 1 /- 3	+ 2 / 0	+ 0 /- 1	+ 0 /- 1
e/μ Energy Resolution	+ 2 /- 2	+ 0 /- 4	+ 0 /- 1	+ 1 /- 1
e/μ Scale Factor	+ 7 /- 6	+ 0 /- 3	+ 4 /- 4	+ 4 /- 3
Jet Energy Scale	+ 8 /-12	+11 /- 4	+ 4 /- 3	+ 5 /- 5
JER	+ 4 /- 4	+ 0 /- 4	+ 0 /- 1	+ 2 /- 2
DY Method	+ 2 /- 2	+ 0 /- 3	+ 0 / 0	+ 2 / 0
Fake	+ 4 /- 4	+ 0 /- 4	+ 3 /- 3	+ 2 /- 1
b-tag efficiency	+ 9 /- 5	+10 /- 5	+ 8 /- 5	+ 8 /- 6
l-tag efficiency	+ 1 /- 1	+ 0 /- 3	+ 1 /- 1	+ 1 /- 1
Generator	+ 1 /- 1	+ 0 /- 3	+ 1 /- 1	+ 1 /- 1
Parton Shower	+ 3 /- 2	+ 0 / 0	+ 4 /- 3	+ 3 /- 2
ISR	+ 2 /- 1	+ 0 /- 3	+ 1 /- 1	+ 1 /- 1
FSR	+ 5 /- 3	+ 4 /- 4	+ 1 /- 1	+ 2 /- 2
PDF	+ 3 /- 2	+ 3 /- 3	+ 3 /- 2	+ 3 /- 2
Pile-up	+ 3 /- 3	+ 2 /- 5	+ 1 /- 1	+ 2 /- 2
MC Cross Section	+ 1 /- 1	+ 0 /- 3	+ 1 /- 1	+ 1 /- 1
All systematics	+19 /-17	+19 /-12	+13 /- 9	+13 /-10
Stat. + Syst.	+40 /-34	+34 /-27	+21 /-18	+19 /-16

Table 11: The $t\bar{t}$ cross section uncertainties for the b-tagging analysis. The labels are defined in the caption of Table 5.

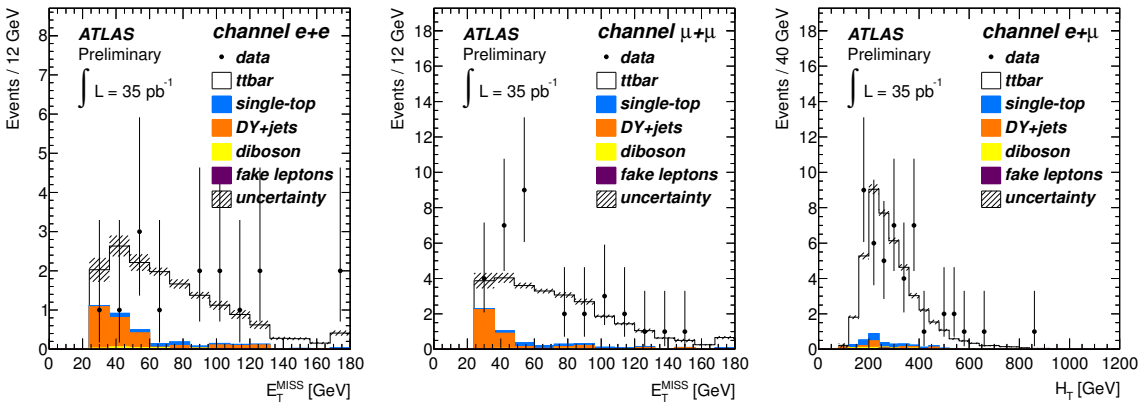

(a) (b) (c)

Figure 6: The $E_{\mathrm{T}}^{\mathrm{miss}}$ distributions for the ee and $\mu\mu$ channels and the H_{T} distribution for the $e\mu$ channel, in each case after b-tagging has been applied.

Channel	$\sigma_{t\bar{t}}$ (pb) (stat., syst., lumi.)
ee	$163\ ^{+57}_{-48}\ ^{+31}_{-27}\ ^{+8}_{-5}$
$\mu\mu$	$185\ ^{+51}_{-45}\ ^{+34}_{-21}\ ^{+8}_{-7}$
$e\mu$	$162\ ^{+28}_{-25}\ ^{+19}_{-14}\ ^{+7}_{-5}$
Combined	$171\ \pm 22\ ^{+21}_{-16}\ ^{+7}_{-6}$

Table 12: Measured cross sections for the b-tagging baseline analysis in each individual dilepton channel, and all three channels combined. The uncertainties are obtained from the likelihood minimization.

(ϵ_b) using Monte-Carlo and other data-driven techniques.

Ideally, top quark pair events produce exactly two b-jets, assuming that the top quark decays 100% into the Wb final state. If only b-jets were tagged, then the expected number of events with two b-tagged jets is $N_{sig} \cdot \epsilon_b^2$, and with one b tagged is $2N_{sig} \cdot \epsilon_b(1-\epsilon_b)$, where N_{sig} is the number of $t\bar{t}$ signal events. However, the number of b-jets varies since b-jets from top quark decays can be out of acceptance or additional b-jets are produced through gluon radiation and gluon splitting. Moreover, c-jets and light jets in the event can also be tagged.

These effects are taken into account by defining the fractions (F_{ijk}) of events containing i b-jets, j c-jets and k light jets after applying the event selection requirements. The F_{ijk} are estimated from MC simulation and background calculations. The largest F_{ijk} are for events with two b-jets and with two to four observed jets, representing almost 70% of the total expected events. The next largest source is events with one b-jet with two to four observed jets, representing almost 20% of the total. The expected distribution of tags in an event, $< N_n >$, can be calculated by combining all possible contributions taking into account these fractions:

$$< N_n >= \sum_{i,j,k} \Big\{ [\sigma_{t\bar{t}} \cdot BR \cdot A_{t\bar{t}} \cdot L \cdot F_{ijk}^{t\bar{t}} + N_{Z+\text{jets}} F_{ijk}^{Z+\text{jets}} + N_{\text{other}} \cdot F_{ijk}^{\text{other}}] \times \sum_{i'+j'+k'=n} C_i^{i'} \epsilon_b^{i'} (1-\epsilon_b)^{i-i'} \cdot C_j^{j'} \epsilon_c^{j'} (1-\epsilon_c)^{j-j'} \cdot C_k^{k'} \epsilon_l^{k'} (1-\epsilon_l)^{k-k'} \Big\}. \quad (6)$$

In this equation, $A_i^{i'}$ is the number of possible arrangements $\frac{i!}{i'!\cdot(i-i')!}$, and i' is the number of tagged jets of a given flavour while i is the number of jets before applying b-tagging. The parameter BR is the branching ratio to the corresponding channel, $A_{t\bar{t}}$ is the $t\bar{t}$ acceptance and L is the integrated luminosity. The parameters $N_{Z+\text{jets}}$ and N_{other} are the expected numbers of Z/γ^*+jets and other background events.

The selection of dilepton candidate events in this analysis is identical to that of the baseline analysis without b-tagging described in Section 4.2. The SV0 b-tagging algorithm [27] is used to b-tag the jets using an operating point that has a nominal b-tagging efficiency of about 50%. The backgrounds are estimated in the same way as the baseline analysis without b-tagging with the exception of the $Z + b\bar{b}$ final state. This background is obtained from MC calculations and a systematic uncertainty of 100% on its rate is assigned; it represents less than 10% of the total Drell-Yan background contribution. These background estimates are shown in Fig. 7.

The distribution of the number of tags in a given event, N_n, is used to simultaneously determine the b-tagging efficiency and the $t\bar{t}$ cross section. Equation 6 is used in a likelihood fit of the observed N_n distributions in the three channels to predict the number of b-tagged jets as a function of the b-tagging efficiency and $t\bar{t}$ cross section.

The results for the individual and combined cross section measurements are shown in Fig. 7 and summarized in Table 13. These are in good agreement with the baseline measurements. The complete results

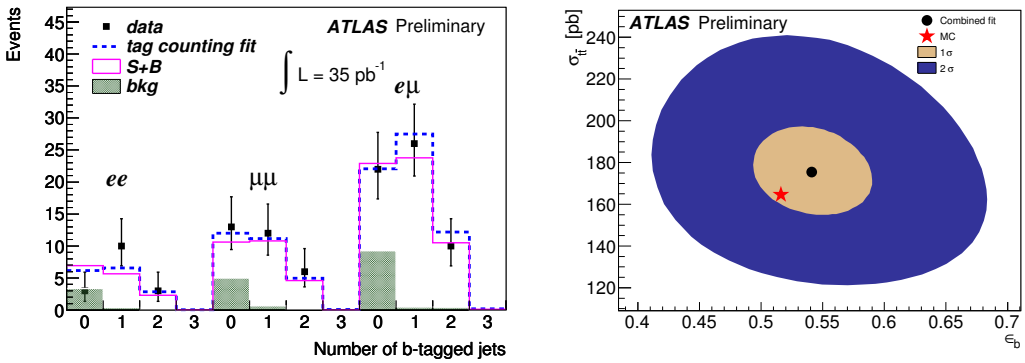

Figure 7: Fitted and observed b-tagged jet multiplicity distribution showing the signal and background contributions (a) and the contour for the measured b-tagging efficiency and $t\bar{t}$ cross section when combining the ee, $\mu\mu$ and $e\mu$ final states (b).

Channel	$\sigma_{t\bar{t}}$ (pb) (stat., syst., lumi.)
ee	$196\,^{+63}_{-52}\,^{+28}_{-25}\,\pm 7$
$\mu\mu$	$197\,^{+49}_{-43}\,^{+25}_{-22}\,\pm 7$
$e\mu$	$162\,^{+27}_{-25}\,\pm 16\,\pm 6$
Combined	$176 \pm 22 \pm 22 \pm 6$

Table 13: Measured cross sections for the simultaneous measurement of the cross section and b-tagging efficiency for the three dilepton channels, and the all three channels combined. The uncertainties are obtained from the likelihood minimization.

of the likelihood fit are shown in Table 14, which summarizes the measured values and the uncertainties for the b-tagging efficiency and $t\bar{t}$ cross section measurements.

	ee	$\mu\mu$	$e\mu$	Combined
Fit Result for ϵ_b (%)	63	55	51	54
Ratio of Fit to MC	1.23	1.06	0.99	1.05
Relative Statistical Uncertainty (%)	±18	±18	±12	±9.1
Systematic Uncertainties	$\delta\epsilon_b/\epsilon_b$ (%)			
Charm & Light Quark Tagging Efficiency	0.4	0.4	0.4	0.4
Background Normalization	3.8	8.3	3.5	3.9
Flavour Composition	2.1	2.1	1.5	1.7
Total Systematic Uncertainty on ϵ_b	4.3	8.6	3.8	4.3
Stat.+Syst.	±19	±20	±13	±10
$\sigma_{t\bar{t}}$ (pb)	196	197	162	176
Relative Statistical Uncertainty (%)	+32/-27	+25/-22	+17/-15	12
Systematic Uncertainties	$\delta\sigma_{tt}/\sigma_{tt}$ (%)			
Selection Acceptance	11	7	8	10
Charm & Light Quark Tagging Efficiency	0.4	0.4	0.4	0.4
Background Normalization	6.0	9.3	5.5	6.3
Flavour Composition	1.7	1.7	1.5	1.6
Total Systematic Uncertainty on $\sigma_{t\bar{t}}$	±13	±12	±10	±12
Luminosity	3.4	3.4	3.4	3.4
Stat.+Syst.+Luminosity	+35/-30	+28/-25	+20/-18	+17/-16

Table 14: Summary of the results and uncertainties for the simultaneous measurement of the b-tagging efficiency and $t\bar{t}$ cross section.

8 Summary

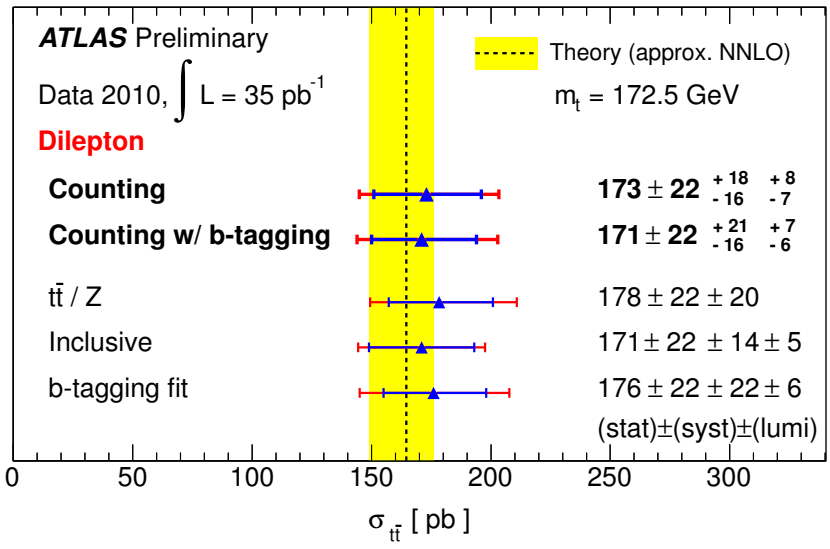

Figure 8: The $\sigma_{t\bar{t}}$ cross section measurements presented in the note. The bold-faced measurements are the results of the two baseline analyses. The yellow bar reflects the uncertainty on the theoretical prediction, which includes some of the NNLO corrections supplemented by soft gluon resummation at the next-to-next-to-leading-logarithm accuracy.

We have summarized measurements of the $t\bar{t}$ production cross section in dilepton final states produced in pp collisions at the Large Hadron Collider.

The baseline analysis that performs a kinematic selection and counts the number of events in the ee, $\mu\mu$ and $e\mu$ final states results in

$$\sigma_{t\bar{t}} = 173 \pm 22(\text{stat.})^{+18}_{-16}(\text{syst.})^{+8}_{-7}(\text{lum.})\ \text{pb}.$$

Extensions of the counting method presented in the note are an analysis in which the $\sigma_{t\bar{t}}$ measurement is normalized using the Z cross section to reduce systematic uncertainties, and an inclusive dilepton analysis.

We also performed a b-tagging baseline counting measurement requiring at least one b-tagged jet with less restrictive kinematic requirements. This results in a cross section measurement of

$$\sigma_{t\bar{t}} = 171 \pm 22(\text{stat.})^{+21}_{-16}(\text{syst.})^{+7}_{-6}(\text{lum.})\ \text{pb}.$$

This measurement was cross-checked with a complementary analysis that simultaneously measured $\sigma_{t\bar{t}}$ and the b-tagging efficiency.

The $\sigma_{t\bar{t}}$ cross section measurements presented in the note are summarized in Figure 8. We note that these measurements are strongly correlated as they are based on the same data sample. They are in very good agreement with the expected results from SM $t\bar{t}$ production predictions.

References

[1] S. L. Glashow, Nucl. Phys. **22** (1961) 579; S. Weinberg, Phys. Rev. Lett. **19** (1967) 1264; A. Salam, Elementary Particle Theory, ed. N. Svartholm, (Almqvist and Wiksell, Stockholm, 1968), p. 367.

[2] S. Moch and P. Uwer, Theoretical status and prospects for top-quark pair production at hadron colliders, Phys. Rev. D78 (2008) 034003, arXiv:0804.1476 [hep-ph];
U. Langenfeld, S. Moch, and P. Uwer, New results for $t\bar{t}$ production at hadron colliders, arXiv:0907.2527 [hep-ph]. Accepted for publication in Eur. Phys. J. C.

[3] ATLAS Collaboration, arXiv:1012.1792 [hep-ex], accepted to Eur. Phys. Journal C

[4] CMS Collaboration, arXiv:1010.5994 [hep-ex].

[5] ATLAS Collaboration, Updated Luminosity Determination in pp Collisions at $\sqrt{s} = 7$ TeV using the ATLAS Detector ATLAS-CONF-2011-034, http://cdsweb.cern.ch/record/1334563.

[6] ATLAS Collaboration, ATLAS Experiment at the CERN Large Hadron Collider, JINST 3 S08003 (2008).

[7] S. Agostinelli, et al., Geant4 – a simulation toolkit, Nucl. Instrum. Meth. A 506 (2003) 250;
J. Allison, et al., Geant4 developments and applications, IEEE Transactions on Nuclear Science 53 No. 1 (2006) 270–278.

[8] ATLAS Collaboration, The ATLAS Simulation Infrastructure, Eur. Phys. J. C **70** (2010) 823, arXiv:1005.4568.

[9] S. Frixione and B. R. Webber, Matching NLO QCD computations and parton shower simulations, JHEP 06 (2002) 029, arXiv:hep-ph/0204244;
S. Frixione, P. Nason and B. R. Webber, Matching NLO QCD and parton showers in heavy flavour production, JHEP 08 (2003) 007, arXiv:hep-ph/0305252;
S. Frixione, E. Laenen and P. Motylinski, Single-top production in MC@NLO, JHEP 03 (2006) 092, arXiv:hep-ph/0512250.
To generate $t\bar{t}$ events v3.41 was used.

[10] P. M. Nadolsky et al., Implications of CTEQ global analysis for collider observables, Phys. Rev. D78 (2008) 013004, arXiv:0802.0007 [hep-ph].

[11] M. Aliev, H. Lacker, U. Langenfeld, S. Moch, and P. Uwer, *HATHOR*, http://www.physik.huberlin.de/pep/tools.

[12] S. Frixione, E. Laenen, P. Motylinski, B. R. Webber and C. D. White, Single-top hadroproduction in association with a W boson, JHEP**07** (2008) 029, arXiv:0805.3067 [hep-ph].

[13] M. L. Mangano, M. Moretti, F. Piccinini, R. Pittau and A. D. Polosa, ALPGEN, a generator for hard multiparton processes in hadronic collisions, JHEP 07 (2003) 001, arXiv:hep-ph/0206293. To generate W+jets, Z/γ^*+jets, and QCD multi-jet events v2.13 was used.

[14] J. Pumplin et al., New generation of parton distributions with uncertainties from global QCD analysis, JHEP 07 (2002) 012, arXiv:hep-ph/0201195.

[15] ATLAS Collaboration, Expected Performance of the ATLAS Experiment: Detector, Trigger and Physics, CERN-OPEN-2008-020, arXiv:0901.0512 [hep-ex], pages 874–881.

[16] R. Hamberg, W. L. van Neerven, and T. Matsuura, A complete calculation of the order α_s^2 correction to the Drell-Yan K factor, Nucl. Phys. B359 (1991) 343; Erratum-ibid. B644 (2002) 403.
C. Anastasiou, L. J. Dixon, K. Melnikov, and F. Petriello, High precision QCD at hadron colliders: Electroweak gauge boson rapidity distributions at NNLO, Phys. Rev. D69 (2004) 094008.

[17] G. Corcella et al., HERWIG 6.5: an event generator for Hadron Emission Reactions With Interfering Gluons (including supersymmetric processes), JHEP 01 (2001) 010, arXiv:hep-ph/0011363; G. Corcella et al., HERWIG 6.5 release notes, arXiv:hep-ph/0210213.

[18] J. M. Butterworth et al., Multiparton interactions in photoproduction at HERA, Z. Phys. C72 (1996) 637.

[19] J. M. Campbell and R. K. Ellis, An update on vector boson pair production at hadron colliders, Phys. Rev. **D60** (1999) 113006.

[20] P. Nason, A new method for combining NLO QCD with shower Monte-Carlo algorithms, JHEP 11546 (2004) 040, arXiv:hep-ph/0409146.

[21] B. P. Kersevan and E. Richter-Was, The Monte-Carlo event generator AcerMC version 2.0 with interfaces to PYTHIA 6.2 and HERWIG 6.5, arXiv:hep-ph/0405247.

[22] ATLAS Collaboration, Measurement of the $W \to \ell\nu$ and $Z/\gamma^* \to \ell\ell$ production cross sections in proton-proton collisions at $\sqrt{s} = 7$ TeV with the ATLAS detector, JHEP 12 (2010) 060, arXiv:1010.2130.

[23] M. Cacciari, G. P. Salam and G. Soyez, The anti-kt jet clustering algorithm, JHEP 0804 (2008) 063, arXiv:0802.1189 [hep-ph].

[24] ATLAS Collaboration, Measurement of inclusive jet and dijet cross sections in proton-proton collisions at 7 TeV centre-of-mass energy with the ATLAS detector, to be submitted to Eur. Phys. J. C 71 (2011) 1, arXiv:1009.5908v2 [hep-ex].

[25] ATLAS Collaboration, Data-Quality Requirements and Event Cleaning for Jets and Missing Transverse Energy Reconstruction with the ATLAS Detector in Proton-Proton Collisions at a Center-of-Mass Energy of $\sqrt{s} = 7$ TeV, ATLAS-CONF-2010-038.

[26] ATLAS Collaboration, Impact Parameter-Based b-Tagging Algorithms in the 7 TeV Collision Data with the ATLAS Detector: the TrackCounting and JetProb Algorithms, ATLAS-CONF-2010-041.

[27] ATLAS Collaboration, Callibrating the b-Tag and Misstag Efficiencies of the SV0 b-Tagging Algorithm with 3 pb^{-1} of Data with the ATLAS Detector, ATLAS-CONF-2010-099.

[28] C. G. Lester and D. J. Summers, Measuring masses of semi-invisibly decaying particles pair produced at hadron colliders, Phys. Lett. **B463** (1999), 99–103.

[29] CDF Collaboration, T, Aaltonen *et al.*, First Measurement of the Ratio $\sigma_{t\bar{t}}/\sigma_{Z/\gamma}$ and Precise Extraction of the $t\bar{t}$ Cross Section, Phys. Rev. Lett. **105** (2010), 012001, arXiv:1004.3224 [hep-ex].

[30] ATLAS Collaboration, Measurement of the WW production cross section in proton-proton collisions at $\sqrt{s} = 7$ TeV with the ATLAS detector, ATLAS-CONF-2011-015.

[31] CMS Collaboration, First Measurement of W+W- production and Search for Higgs Boson in pp Collisions at $\sqrt{s} = 7$ TeV, CERN-PH-EP-2011-015; CMS-EWK-10-009-004.

9 Extra plots

9.1 $e\mu$ control sample

The τ leptons decay to e and μ only a fraction of the time and some of their momentum is carried off by neutrinos, so that the $Z \to \tau^+\tau^-$ process lacks the large and easily identifiable peak in dilepton invariant mass distribution. However, a signature can be found in which $Z \to \tau^+\tau^-$ is the largest contribution, which allow us to check its normalization and kinematics. After the selection of $e\mu$ channel events, but with exactly zero jets, there is no large contribution from $Z \to ee$ and $Z \to \mu\mu$, making the $Z \to \tau^+\tau^- \to e\mu + \nu\nu\nu\nu$ visible, see Figure 9.

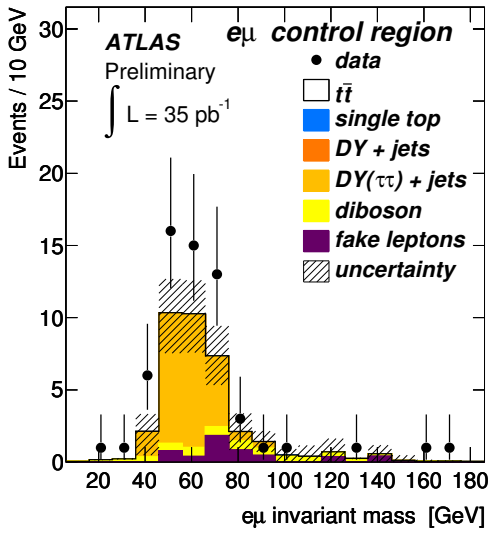

Figure 9: Data and backgrounds in the $e\mu$ channel with exactly zero reconstructed jets, where $Z \to \tau^+\tau^-$ is the largest expected source.

9.2 Templates used for the inclusive dilepton analysis

For the inclusive dilepton analysis (Section 6.2.2), the two-dimensional parameter space defined by $E_{\mathrm{T}}^{\mathrm{miss}}$ and $\mathrm{N_{jets}}$ is used to naturally separate WW, $Z \to \tau\tau$ and $t\bar{t}$ dilepton contributions, and fit the observed data to Monte-Carlo generated templates of all expected processes, see Figure 10 for the Monte-Carlo templates.

9.3 Cross section with Z normalization

Figure 11 shows the distribution of the variable $r = n_{Z\to\ell}/n_{\bar{t}t\to ll}$ described in Section 6.2.1 and the contour resulting from the 2D fit to the integrated luminosity and the $t\bar{t}$ cross section.

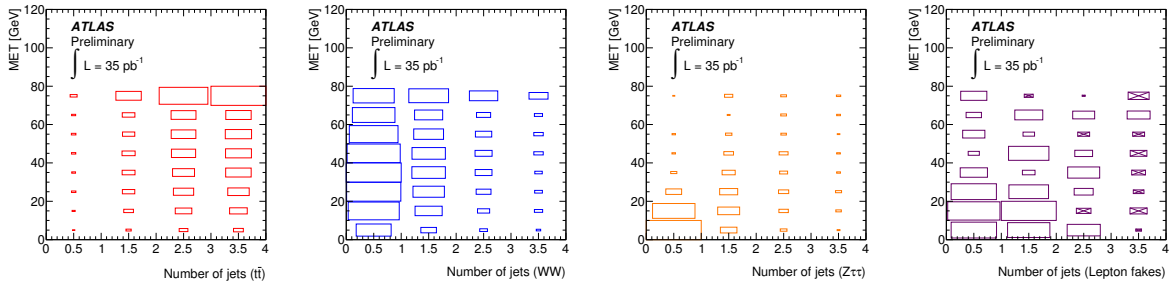

(a) (b) (c) (d)

Figure 10: Event distributions in the jet multiplicity and $E_{\mathrm{T}}^{\mathrm{miss}}$ plane in the $e\mu$ channel for the expected dominating sources.

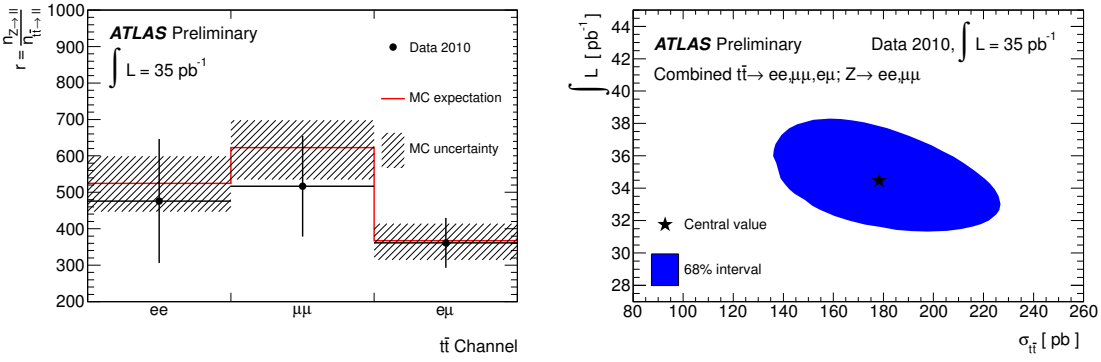

(a) (b)

Figure 11: (a) Distribution of $r = \frac{n_{Z\to ll}}{n_{t\bar{t}\to ll}}$ for the three $t\bar{t}$ analysis channels. For the $e\mu$ channel $n_{Z\to ll} = 2 \times \sqrt{n_{Z\to ee} \times n_{Z\to \mu\mu}}$. The data are compared with the expectation from the MC. (b) Result of the $t\bar{t}$ / Z cross section extraction in the 2D luminosity and $t\bar{t}$ cross section plane. The point shows the central value of the fit and the shaded area is the 68% interval.